Experimental verification of power-law non-Newtonian axisymmetric porous gravity currents, JFM Rapids DOI: 10.1017/jfm.2013.389

Sandro Longo†, Vittorio Di Federico
Luca Chiapponi, Renata Archetti

Supplementary Material

1. Uncertainty analysis

In order to check the experiments against the theory, we estimated the uncertainties in the experimental data and the 95% confidence limits of the model. The height of the intruding current h is expressed as a function of the radius r and time t, with six parameters involved:

$$h = h\left(r, t, m, n, \Delta\rho, Q, d, \phi\right). \qquad (1.1)$$

The uncertainty in a parameter, expressed by the standard deviation, gives a contribution to the uncertainty in h equal to:

$$\frac{\partial h}{\partial m}\sigma_m, \ \frac{\partial h}{\partial n}\sigma_n, \dots, \qquad (1.2)$$

where σ_m is the standard deviation of m. We assumed that gravity is fixed and invariable and α is exempt from uncertainty. The total uncertainty in h is obtained by combining in quadrature the contribution of the uncertainties in the parameters:

$$\sigma_h^2 = \left(\frac{\partial h}{\partial m}\right)^2 \sigma_m^2 + \left(\frac{\partial h}{\partial n}\right)^2 \sigma_n^2 + \dots . \qquad (1.3)$$

Figure 1 shows the contributions of the uncertainties in the six parameters and figure 2 shows in detail the 95% confidence limits and the error bars (two standard deviations) for Test 11. Note that the difference between the estimation of the experimental points and the theoretical profile contains the zero, hence experimental data and the theoretical profile are statistically equal with a 95% level of confidence.

The uncertainties in the parameters were obtained by means of a statistical analysis of the rheometric data, by manufacturer's specifications for the glass beads or on the other instruments adopted. A coefficient of variation equal to 1% was assumed for the porosity.

The rheometric data were evaluated independently from rheometric tests. Since the power-law model is a local approximation, the range of shear rate included in the regression analysis is a key parameter in deriving the values of m and n. A suggestion on this range could be obtained by estimating the shear rate at porous scale (see eq.(4.1); for the velocity u we used the average velocity in the vertical, coherently with the model assumptions). Eq.(4.1) provides only an estimate of the shear rate, but the local shear

† Email address for correspondence: sandro.longo@unipr.it
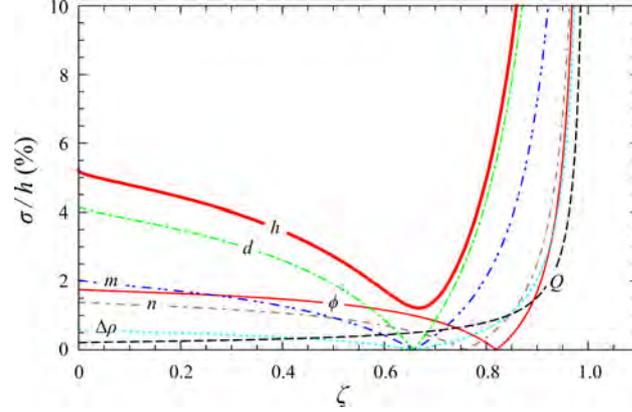
FIGURE 1. Coefficient of variation, σ_h/h, and the contribution due to the uncertainty in the six parameters. Test 11, $t = 14'\,30''$.
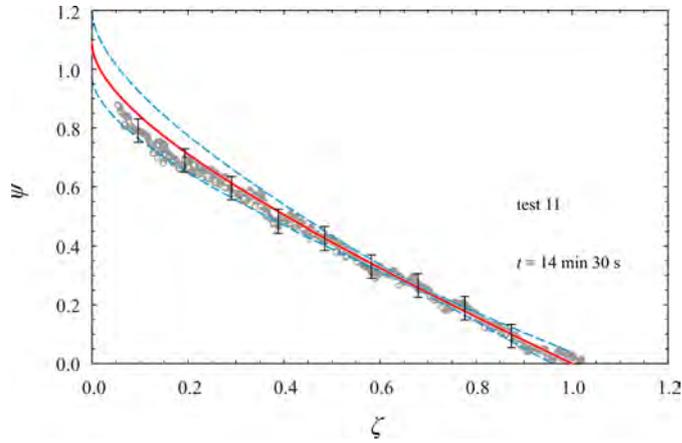

FIGURE 2. Test 11, theoretical profile (bold red curve) and 95% confidence limits (dashed blue curves). The error bars indicate $\pm$ twice the uncertainty in detecting the boundary between the intruding current and the ambient fluid.

rate can be much larger, hence we decided to fit the rheometric data in a wider range. Indeed the optimisation algorithm tends to reproduce the parameters obtained fitting the rheometric data in the narrow range of shear rate, but it cannot be conclusive, since other sources of uncertainties (i.e. in the parameters $d, Q, \Delta\rho, \phi$) are not included in the algorithm.

The other figures show the same data reported in figure 1 for all remaining tests (except Test 9 and 10 with water as ambient fluid) at the time correspondent to the last available shot. It is seen that the same conclusions derived for Test 11 may be drawn for all other tests.
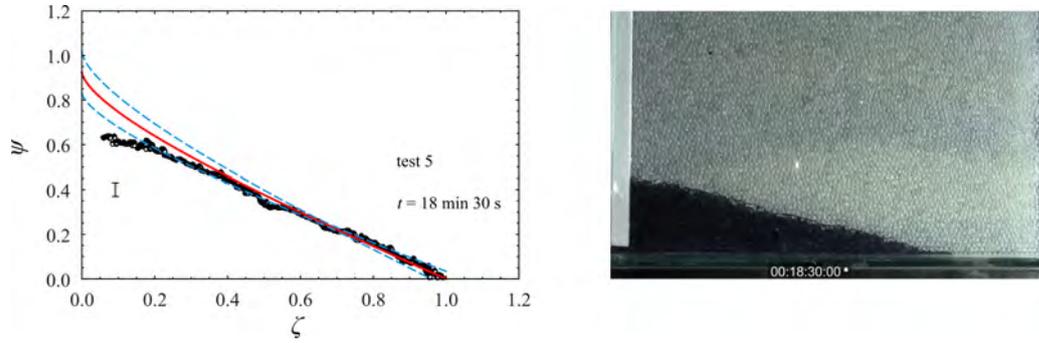
FIGURE 3. Test 5, $m = 0.68 \pm 3.5\%$ Pa·s^n, $n = 0.35 \pm 3.5\%$, $\Delta\rho = 1175 \pm 1.0\%$ kg·m^{-3}, $Q = 0.60 \pm 1.0\%$ ml·s^{-1}, $\alpha = 1.0$, $d = 3.0 \pm 5\%$ mm, $\phi = 0.38 \pm 1\%$. The error bar and the confidence limits (dashed blue curves) refer to 95% confidence level.
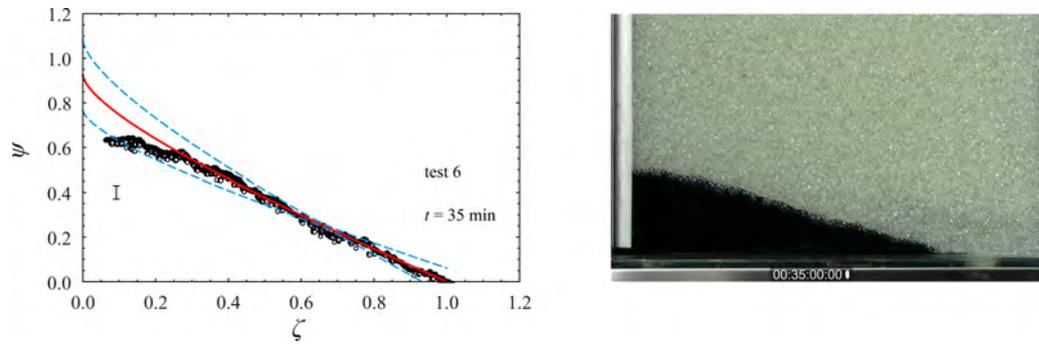

FIGURE 4. Test 6, $m = 0.68 \pm 3.5\%$ Pa·s^n, $n = 0.35 \pm 3.5\%$, $\Delta\rho = 1175 \pm 1.0\%$ kg·m^{-3}, $Q = 0.32 \pm 1.0\%$ ml·s^{-1}, $\alpha = 1.0$, $d = 2.0 \pm 10\%$ mm, $\phi = 0.38 \pm 1\%$.
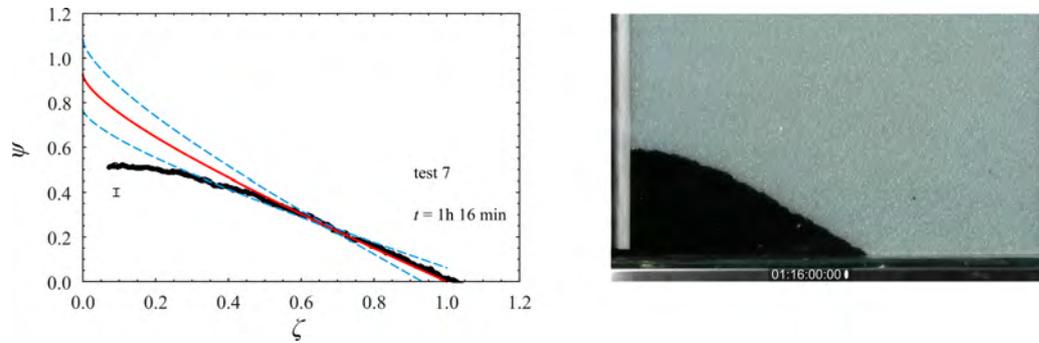
FIGURE 5. Test 7, $m = 0.80 \pm 3.5\%$ Pa·s^n, $n = 0.33 \pm 3.5\%$, $\Delta\rho = 1169 \pm 1.0\%$ kg·m^{-3}, $Q = 0.15 \pm 1.0\%$ ml·s^{-1}, $\alpha = 1.0$, $d = 1.0 \pm 10\%$ mm, $\phi = 0.38 \pm 1\%$.
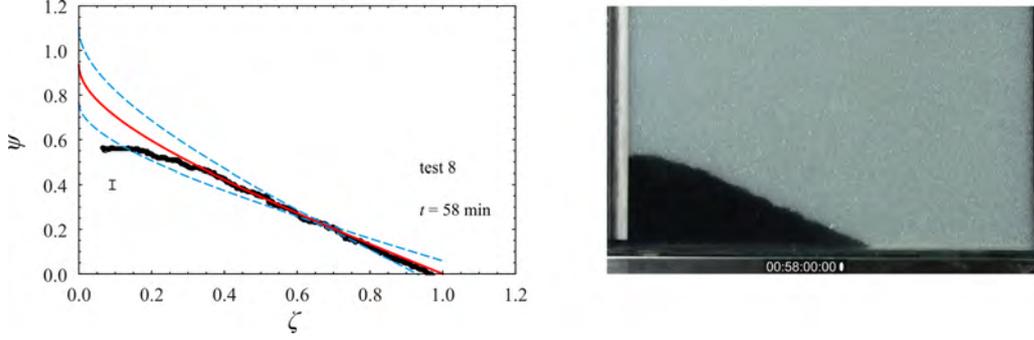
FIGURE 6. Test 8, $m = 0.33 \pm 3.5\%$ Pa·s^n, $n = 0.48 \pm 3.5\%$, $\Delta\rho = 1000 \pm 1.0\%$ kg·m^{-3}, $Q = 0.20 \pm 1.0\%$ ml·s^{-1}, $\alpha = 1.0$, $d = 1.0 \pm 10\%$ mm, $\phi = 0.38 \pm 1\%$.
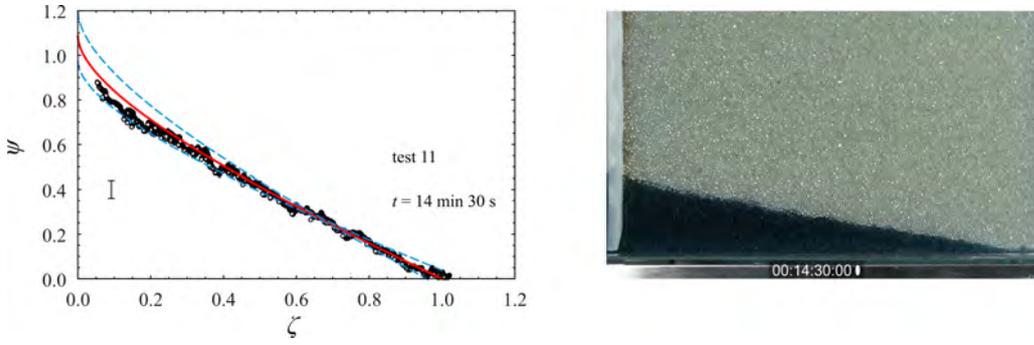

FIGURE 7. Test 11, $m = 0.12 \pm 3.5\%$ Pa·s^n, $n = 0.43 \pm 3.5\%$, $\Delta\rho = 1000 \pm 1.0\%$ kg·m^{-3}, $Q = (0.06 \pm 0.5\%) \cdot t^{1/2}$ ml·s^{-1}, $\alpha = 1.5$, $d = 2.0 \pm 10\%$ mm, $\phi = 0.38 \pm 1\%$.
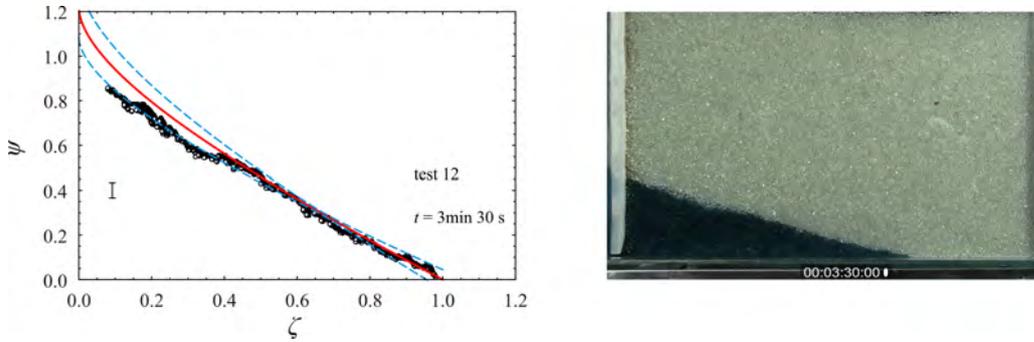

FIGURE 8. Test 12, $m = 0.12 \pm 3.5\%$ Pa·s^n, $n = 0.43 \pm 3.5\%$, $\Delta\rho = 1000 \pm 1.0\%$ kg·m^{-3}, $Q = (0.032 \pm 0.5\%) \cdot t$ ml·s^{-1}, $\alpha = 2.0$, $d = 2.0 \pm 10\%$ mm, $\phi = 0.38 \pm 1\%$.
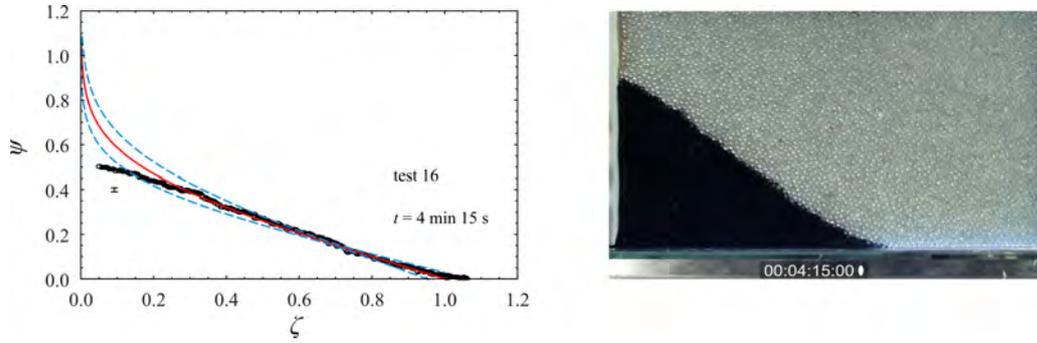
FIGURE 9. Test 16, $m = 0.58 \pm 3.5\%$ Pa·s^n, $n = 1.0 \pm 3.5\%$, $\Delta\rho = 1250 \pm 1.0\%$ kg·m^{-3}, $Q = (4.0 \pm 0.5\%)$ ml·s^{-1}, $\alpha = 1.0$, $d = 3.0 \pm 5\%$ mm, $\phi = 0.38 \pm 1\%$.
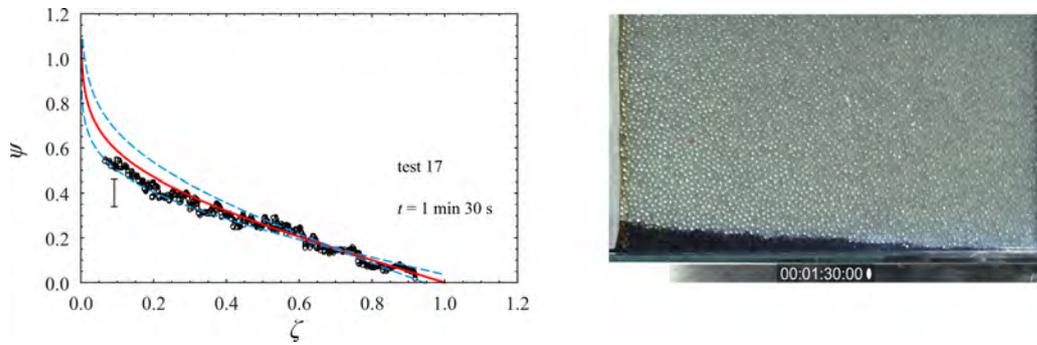
FIGURE 10. Test 17, $m = 0.012 \pm 3.5\%$ Pa·s^n, $n = 1.0 \pm 3.5\%$, $\Delta\rho = 1145 \pm 1.0\%$ kg·m^{-3}, $Q = (4.0 \pm 0.5\%)$ ml·s^{-1}, $\alpha = 1.0$, $d = 3.0 \pm 5\%$ mm, $\phi = 0.38 \pm 1\%$.
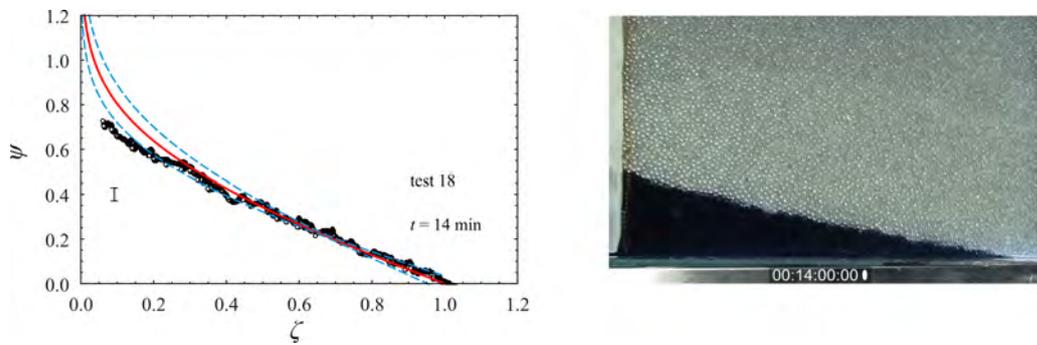
FIGURE 11. Test 18, $m = 0.26 \pm 3.5\%$ Pa·s^n, $n = 1.0 \pm 3.5\%$, $\Delta\rho = 1241 \pm 1.0\%$ kg·m^{-3}, $Q = (0.06 \pm 0.5\%) \cdot t^{1/2}$ ml·s^{-1}, $\alpha = 1.5$, $d = 3.0 \pm 5\%$ mm, $\phi = 0.38 \pm 1\%$.